Compressible Kolmogorov flow in strongly coupled dusty plasma using molecular dynamics and computational fluid dynamics. II. A comparative study

3 authors:

Akanksha Gupta
Indian Institute of Technology Kanpur
15 PUBLICATIONS **37** CITATIONS

SEE PROFILE

Rajaraman Ganesh
Institute for Plasma Research
124 PUBLICATIONS **480** CITATIONS

SEE PROFILE

Ashwin Joy
Institute for Plasma Research
23 PUBLICATIONS **214** CITATIONS

SEE PROFILE

Some of the authors of this publication are also working on these related projects:

Multi-cusp Plasma Device View project

Project title : A first principle numerical simulation of strongly coupled multi ion plasma in the presence of an external magnetic field View project

Kolmogorov flow in two dimensional strongly coupled Yukawa liquid: A molecular dynamics study

Akanksha Gupta, Rajaraman Ganesh, and Ashwin Joy

View Online   Export Citation   CrossMark

ARTICLES YOU MAY BE INTERESTED IN

AIP
Publishing

Kolmogorov flow in two dimensional strongly coupled Yukawa liquid: A molecular dynamics study

Akanksha Gupta, Rajaraman Ganesh,[a)] and Ashwin Joy
Institute for Plasma Research, Bhat, Gandhinagar, Gujarat 382428, India

The transition from laminar to turbulent flows in liquids remains a problem of great interest despite decades of intensive research. Here, we report an atomistic study of this transition in a model Yukawa liquid using molecular dynamics simulations. Starting from an thermally equilibrated Yukawa liquid, for a given value of coupling parameter Γ (defined as ratio of potential energy to kinetic energy per particle) and screening length κ, a subsonic flow of magnitude U_0 is superposed and transition to an unstable regime is observed eventually leading to turbulent flow at sufficiently high Reynolds numbers. We have performed a parametric study for a range of Reynolds number R and found that the flow is neutrally stable for $R < R_c(\Gamma)$, while a transition from laminar to turbulent flow occurs for $R > R_c(\Gamma)$, where R_c is the critical value of Reynolds number. Strong molecular shear heating is observed in all cases studied here. It is found that the coupling parameter Γ decreases because of molecular shear heating on a time scale comparable to the instability time scale. Irrespective of the initial value of coupling parameter Γ, the average heating rate is found to be sensitive to the ratio of equilibrium flow speed to the thermal speed, say, $\alpha = \frac{U_0}{v_{th}}$, where $v_{th} = \sqrt{\frac{2}{\Gamma}}$. Our results reported here are expected to be generic and should apply to a wide variety of strongly coupled systems such as laboratory dusty plasma, molten salts, and charged colloidal systems. © 2015 AIP Publishing LLC. [http://dx.doi.org/10.1063/1.4934535]

I. INTRODUCTION

It is well known that micron-sized dust grains immersed in a conventional plasma acquire a high value of charge because of high mobility of electrons.[1] These grains interact with each other via screened Coulomb potential, also known as the Yukawa potential. Screening is because of the background plasma and is characterized by dimensionless screening parameter $\kappa = a/\lambda_D$ (where a is intergrain-spacing and λ_D is Debye length of background plasma). These interacting dust grains behave as a medium which can exhibit solid-like,[2–4] liquid-like,[5] and gas-like[1] features, depending upon screening parameter κ and the value of coupling parameter Γ ($\Gamma = Q_d^2/4\pi\varepsilon_0 a k_B T_d$, wherein Q_d and T_d are charge and temperature of dust grain).

The dynamics of microscopic dust grains can be visualized and tracked (many a times even by unaided eye) by optical cameras in the dusty plasma experiments.[2] Molecular dynamics comes as a powerful tool to study different properties such as phase transition, instability, transport, grain crystallization physics, and also to visualize the dust grains dynamics. For example, in the past, various dynamical properties of dusty plasma determination of transport coefficients, such as shear and bulk viscosities,[6] Maxwell relaxation time (τ_m),[7] heat conduction, wave dispersion,[8] self diffusion[9] and fluid instability like Kelvin-Helmholtz instability,[10] had been addressed using the molecular dynamics simulation.

In an earlier molecular dynamics study,[11] shear heating was identified. In past, macroscopic shear flows have been induced by external laser-drive in Yukawa liquids.[12,13] In one of these experiments,[12] a co-evolving shear heating was observed. However, a detailed study of shear heating in macroscopic flows in Yukawa liquids has not yet been addressed.

In the present work, we consider the well known macroscopic flow, namely, Kolmogorov[14,15] flow [see Fig. 3] as our initial shear flow. Kolmogorov flow is a sinusoidal periodic shear flow, which was first introduced by Russian mathematician Andrey Kolmogorov in 1958–1959. This particular shear flow has been addressed analytically,[14] numerically,[16] and experimentally[15,17] to explore linear, non-linear,[18] and statistical[19] properties of laminar to turbulent transition in fluids.

Using "first principle" molecular dynamics, the early phase and late time dynamics of this hydrodynamic flow in strongly coupled plasma is addressed. We have also performed a parametric study of stability of the flow with Reynolds number R and found that below a critical value of Reynolds number R_c, flow exhibits a neutral stability. However, above $R > R_c$, a transition occurs from laminar to unstable state and eventually turning into a turbulent flow. We observe that for the given value of initial coupling parameter Γ and screening parameter κ, molecular shear heating strongly reduces the magnitude of dynamic coupling parameter and its decay-rate is mainly found to be dependent upon the ratio of equilibrium shear velocity to thermal velocity. We find that the magnitude of coupling parameter decays exponentially by the end of the growth phase, thus altering the state of "background grains" dramatically.

Present paper is organized in the following manner. In Sec. II, we describe the details of molecular dynamics simulation method. In Sec. III, equilibrium profile

a)Electronic mail: ganesh@ipr.res.in

of shear flow and its laminar to turbulent transition are described. In Sec. IV, molecular shear heating effects on coupling strength are described. Finally in Sec. V, we discuss and summarize our present work and indicate future directions.

II. MOLECULAR DYNAMICS SIMULATION

As described in the Introduction, the interaction between grains can be modeled as a Yukawa interaction given by the inter-particle potential energy

$$U(r_{ij}) = \frac{Q_d^2}{4\pi\epsilon_0} \sum_{j\neq i}^{N} \frac{e^{-r_{ij}/\lambda_D}}{r_{ij}}, \tag{1}$$

where $r_{ij} = |r_i - r_j|$ is the distance between ith and jth dust grain. Note that due to fast dynamics of background plasma, we consider plasma properties to be invariant and model only grain dynamics. The N-body problem is then numerically integrated using our parallel code.[20] Time, distance, and energy are normalized to inverse of dust plasma frequency $\sqrt{2}\omega_{pd}^{-1} = \omega_0^{-1}$, mean inter-gain spacing a, and average Coulomb energy of dust particle $\frac{Q_d^2}{4\pi\epsilon_0 a}$, respectively. Hence, all physical quantities appearing henceforth in the paper are dimensionless. In our simulations, the size of the system is decided by average number of dust particles $\bar{n}$. For our choice of $\bar{n} = \frac{1}{\pi}$ and total number of particles $N_d = 62\,500$, $L_x = L_y = L = 443.12$. Screening parameter κ is 0.5. In present work, we do not consider Ewald sums[21] because of sufficiently large system size.

The Yukawa liquid is first thermally equilibrated by connecting the system to a Gaussian thermostat[20] at desired Γ and is evolved for time $t' = 300\omega_0^{-1}$. For next $300\omega_0^{-1}$, the system is isolated from heat-bath and evolved microcanonically. In Fig. 1, the total energy as a function of time is plotted. As can be expected, in the canonical phase (see Fig. 1) a mean energy is attained for a constant value of coupling parameter Γ and in the micro-canonical phase, the total energy is seen to be conserved. However, when shear flow is superimposed over thermally equilibrated dust particles, the total energy changes from 1.147 to 1.3967 (see Fig. 1).

To calculate the "fluid" variables from particle dynamics, a meshgrid of size 55×55 is superimposed on to the system of particles. On an average, each bin would contain $N_b = \frac{N_d}{55 \times 55} \simeq 20$ particles, which is found to be sufficient to estimate average local quantities. We calculate average local "fluid" velocity $\bar{U}(x_G, y_G, t')$, average local vorticity $\bar{\omega}(x_G, y_G, t')$ ($\bar{\omega} = \nabla \times \bar{U}$), average local coupling parameter $\bar{\Gamma}(x_G, y_G, t')$, and average local temperature $\bar{T}(x_G, y_G, t')$ at the grid points, where (x_G, y_G) is the location of a center of a particular bin. For example, average local fluid velocities along x and y directions are calculated as $\bar{U}_x = \frac{1}{N_b} \sum_{i=1}^{N_b} v_{ix}$, $\bar{U}_y = \frac{1}{N_b} \sum_{i=1}^{N_b} v_{iy}$, where v_{ix} and v_{iy} are individual particle velocities along x and y direction. Similarly, average local coupling parameter of grain fluid element velocities is calculated by the following expression:
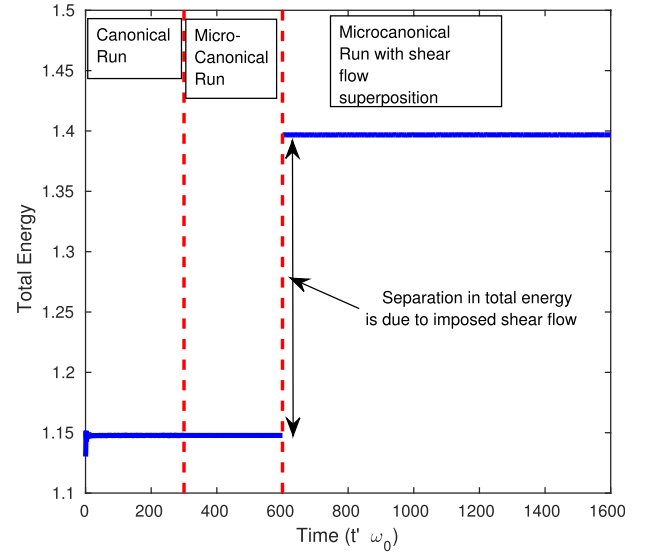

FIG. 1. Total energy vs time plot for coupling parameter $\Gamma_0 = 50$, screening parameter $\kappa = 0.5$, spatial period number $n_0 = 3$ in canonical $(0 - 300)\omega_0^{-1}$ and micro-canonical run $(300 - 600)\omega_0^{-1}$. Next $(600 - 1600)\omega_0^{-1}$ plot is after superposition of shear flow profile over thermally equilibrated dust particles (micro-canonical run). Superposition of shear flow increases the velocity of particles, hence the value of total energy changes from 1.147 to 1.3967 as shown above.

$$\bar{\Gamma}(x_G, y_G, t') = \frac{2}{\frac{1}{N_b} \sum_{i=1}^{N_b} \left[\left(v_{ix}(t') - \overline{U_x} \right)^2 + \left(v_{iy}(t') - \overline{U_y} \right)^2 \right]}. \tag{2}$$

Data shown in Fig. 2 are divided into three regions. In the first region (a), coupling parameter $\bar{\Gamma}(t')$ with time $(0 - 300)\omega_0^{-1}$ has been plotted in canonical phase where thermostat is on, in second region (b), the same variable is plotted against time $(300 - 600)\omega_0^{-1}$ with thermostat off condition (micro-canonical phase). In the last region (c), after superposition of shear flow $U_0(x)\hat{y}$ (see Sec. III for details of shear flow) over system of particle velocities, dynamic coupling parameter $\bar{\Gamma}$ is plotted for time $(600 - 1600)\omega_0^{-1}$. Fig. 2 shows that the coupling parameter is constant before superposition of shear profile however, as shear profile superimposed on thermally equilibrated dust grains and the system is evolved further the value of coupling parameter decays. In Sec. III, we report early and late time behavior of shear flow in strongly correlated Yukawa liquids. Noticeable thing is that shear flow is adiabatic (non-thermostatted) which implies that the heat transfer away from the shear layer is minimal.

III. KOLMOGOROV FLOW AS A INITIAL VALUE PROBLEM IN YUKAWA LIQUID

We have presented in Fig. 3 the equilibrium flow profile of shear flow having spatial periodic number $n_0 = 3$, where the flow is directed towards $\hat{y}$-direction and has transverse shear along $\hat{x}$-direction. In fluid dynamics study such shear flows have been extensively used to understand the laminar to turbulent transition of flows.[14] We superpose shear flow
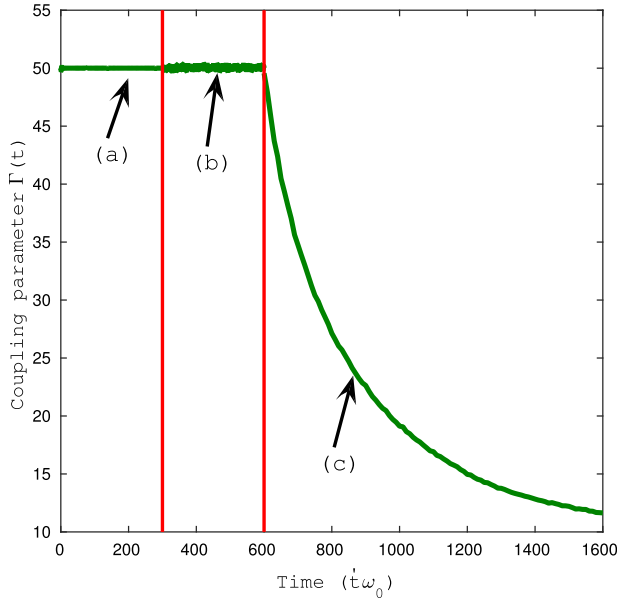
FIG. 2. Average coupling parameter $\bar{\Gamma}(t')$ vs time plot for initial coupling parameter $\Gamma_0 = 50$, screening parameter $\kappa = 0.5$ spatial period number $n_0 = 3$ and shear velocity $U_0 = 1$. (a) canonical run for time $(0 - 300)\omega_0^{-1}$, (b) micro-canonical run for time $(300 - 600)\omega_0^{-1}$, wherein peak to peak fluctuation 1.406%, (c) micro-canonical run for time $(600 - 1600)\omega_0^{-1}$ after superposition of shear flow profile over thermally equilibrated particles of the system.

over thermally equilibrated dust particles at a desired temperature and allow it to evolve micro canonically up to $1000\omega_0^{-1}$ without heat-bath. The initial equilibrium shear flow is $\vec{U}_0(x) = U_0 \cos(\frac{2\pi}{L_x} n_0 x)(1 + \delta \cos(\frac{2\pi}{L_y} my))\hat{y}$, where $U_0 = 1$ (the magnitude of equilibrium velocity, $n_0 = 3$ (spatial period number), $\delta = 0.01$ (magnitude of perturbation), $m = 2$(perturbed mode number). Coupling parameter $\Gamma(t')$ at time $t' = 0$ is $\Gamma_0 = \Gamma(t' = 0) = 50$, for which the thermal velocity $v_{th} = \sqrt{\frac{2}{\Gamma_0}} = 0.2$. It is estimated that the longitudinal sound speed of the system for $\Gamma_0(t' = 0) = 50$ and $\kappa = 0.5$ is with in the range of 2–2.5.[22] Hence, equilibrium velocity ($U_0 = 1$) is greater than thermal speed ($v_{th} = 0.2$) but smaller
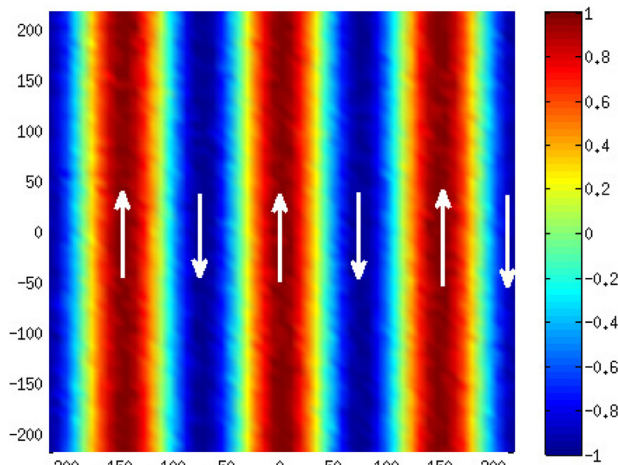
than sound speed ($C_s = 2 - 2.5$) of the system, therefore flow regarded as "subsonic" in nature.

Note that the entire macroscopic flow speed is along $\hat{y}$ direction initially. The transition from laminar to turbulent flow along $\hat{y}$ direction to an unstable macroscopic dynamics state may be identified by calculating the change in perturbed kinetic energy along $\hat{x}$ direction as defined in the following equation:

$$\left| \frac{\delta E_{kin}(t)}{\delta E_{kin}(0)} \right| = \frac{\int \int \left[v_x^2(t) - v_x^2(0) \right] dx dy}{\int \int v_x^2(0) dx dy}. \tag{3}$$

Note that, for convenience, we rewrite time variable t' as $t = t' - 600\omega_0^{-1}$. Henceforth, in the rest of the paper, dynamics will be described with respect to t.

In Fig. 4, perturbed kinetic energy along $x-$direction and coupling parameter is plotted on a log-linear scale against time t. Growth rate of perturbation is found to be approximately equal to 5.5×10^{-2}. In Fig. 4, perturbed kinetic energy along with decay of coupling parameter Γ are plotted in the same figure. A noticeable thing is that the molecular shear heating reduces the value of coupling parameter by 50% ($\Gamma \simeq 26$ at $t = 220\omega_0^{-1}$) from its initial value ($\Gamma_0 = 50$ at $t = 0$). From Fig. 4, it is evident that molecular shear heating is very fast at initial phase of shear flow (before $t = 0$ to $t = 220\omega_0^{-1}$). As observed in Ref. 11, the following two processes are appeared to be at work in the shear region: (a) Decay of coupling parameter or rise in temperature which changes the local viscosity of the system and (b) on macroscale, the free energy in flow shear is released as an instability. Due to this free energy and also because of low viscosity, perturbed modes start to grow. In late time regime, inertial effects dominate over the stabilizing viscous effects. The fluid undergoes laminar to turbulent flow transition, and late time saturation in perturbed kinetic energy is seen. In Fig. 5, we have presented the time evolution of vorticity

FIG. 3. Kolmogorov velocity ($U_0 = 1$) profile in xy plane. White arrows show the direction of local flow along y direction and shear along x direction.
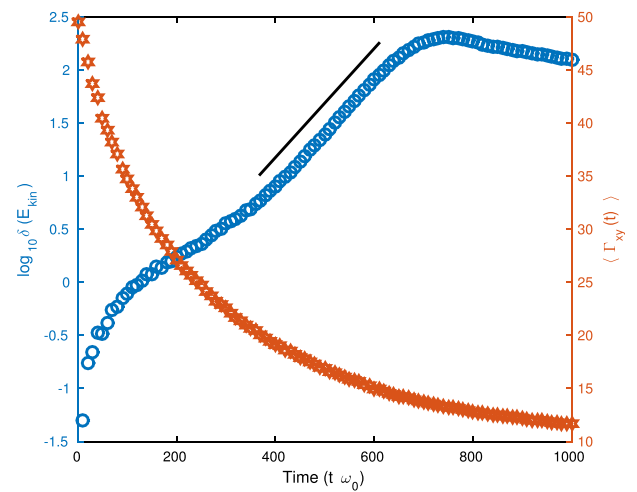

FIG. 4. Perturbed kinetic energy (left y-axis) and decay of coupling parameter (right y-axis) in linear-log scale for number for perturbation mode $m = 2$, initial coupling parameter $\Gamma_0(t = 0) = 50$, screening parameter $\kappa = 0.5$, spatial period number $n_0 = 3$, and shear velocity $U_0 = 1$. Calculated growth rate from simulation is 5.5×10^{-2}.
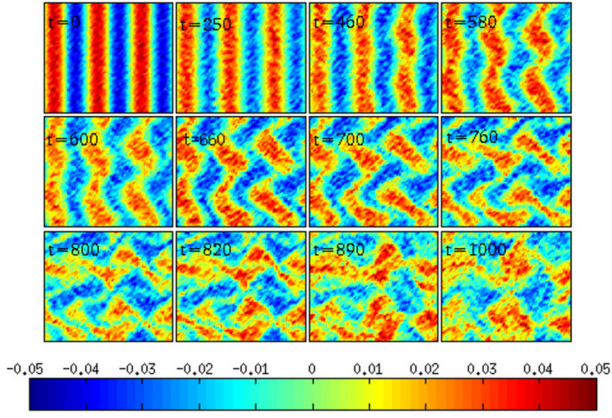
FIG. 5. Fluid vorticity ($\omega = \nabla \times \vec{U}$) contour plots. The grain velocity in the bins is fluidized through a 55×55 grid to construct vorticity. The side color bar shows the magnitude of vorticity and blue and red strips show the opposite sign vorticity, respectively. Perturbation mode $m = 2$, initial coupling parameter $\Gamma_0 = 50$, screening parameter $\kappa = 0.5$ equilibrium spatial period number is $n_0 = 3$, initial Reynolds number $R = 235.149$, and shear velocity $U_0 = 1$. Vorticity plots generated from microscopic velocity show Kolmogorov instability in molecular dynamics; the micro scale heating quickly destroys the vorticity structures.

structure in Yukawa liquid at initial coupling parameter $\Gamma_0 = 50$. As described earlier, to construct these vorticity structures, we first obtain the local velocity by "fluid" dust particle velocities over a 55×55 meshgrid. In vorticity evolution plot [see Fig. 5], it is depicted that in initial time perturbed mode $m = 2$ first grows and in late time mode-mode interaction dominate and nonlinear patterns are obtained. It is found that after some time, vorticity structures are destroyed because of microscale molecular shear heating, the details of which will be discussed in Sec. IV.

In Fig. 6, we have shown results of a parametric study for maximum growth-rate of perturbed mode with initial Reynolds number $R = U_0 l \bar{n} / \eta$, where l and η are the shearing length and initial shear viscosity of the flow, respectively. Here, the value of shear viscosity η is calculated using the Green-Kubo formalism.[7,23] It is depicted in Fig. 6 that for a given value of Γ_0 and κ, flow is neutrally stable below

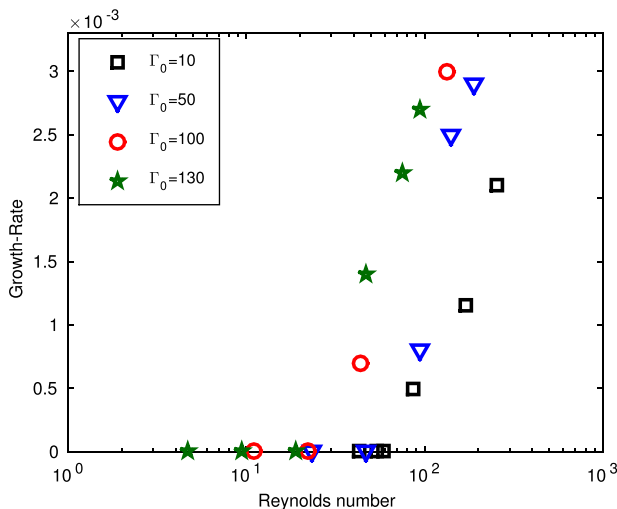FIG. 6. Growth-rate vs initial Reynolds number R plot showing transcritical kind of bifurcation.

$R < R_c$, where R_c is the critical value of Reynolds number and for $R > R_c$ flow becomes unstable and eventually turbulent [see Fig. 6]. It is tempting to speculate from the result shown in Fig. 6 that such laminar to turbulent transition in our system could be a transcritical bifurcation.[24] Interestingly, we find that higher value of coupling parameter Γ decreases the critical value of Reynolds number R_c.

In Sec. IV, we study the effect of viscous heating on shear flow.

IV. MOLECULAR HEATING DUE TO SHEAR FLOW

It is found that, whenever there is a shear in macroscopic velocity profiles, viscous shear heating occurs at the micro-scale. For some fluids, it is not necessary for shear heating to increase the temperature at the shear layer, because heat conduction can be so rapid at the location of the velocity shear where the heat is formed that as soon as heat is generated, it is carried away. Conventionally, the effect of viscous shear heating and thermal conduction is measured by a dimensionless parameter, known as Brinkman number[25,26] $B_r \approx \eta (\Delta V)^2 / \lambda \Delta T$ (where η and λ are shear viscosity and thermal conductivity and ΔV and ΔT are difference in flow velocity and temperature, respectively).[26] Mostly, B_r which is the ratio of viscous heating to thermal conduction is smaller than the unity. The higher is the value of B_r, the lesser will be the heat conduction, and hence, larger the temperature rise near the shear layer. For example, for Taylor-Couette flow in Newtonian and visco-elastic fluids trapped between concentric and rotating cylinders, value of B_r is found to be 0.00359[27] and for conventional water flow in a channel[28] its value is approximately in the range of $(1 - 17) \times 10^{-8}$.

Recently in dusty plasma experiments, using laser driven shear flow study, high temperature peaks are reported[13] in the regions of velocity shear in two-dimensional layer. These high temperature peaks are due to shear heating, which occurs due to collisional scattering at the region of shear location. In such dusty plasma experiments, value of B_r is estimated to be 0.5.[13] We have calculated Brinkman number from our numerical simulation and found that $B_r = 0.9445$ for our system parameters at the grid location $x_G \approx 110$ and time $t = 0$ for $\Gamma_0 = 50$, $\kappa = 0.5$, $\eta(t = 0) = 0.2$ (Ref. 7) and $\lambda(\Gamma_0 = 50, \kappa = 0.5) = 0.4235$,[29,30] the value of ΔT and ΔV are 0.02 and 0.2 from Figs. 7 and 8.

In the shear layers, frequency of collisions between dust grains can be expected to be high. These collisions increase the random thermal velocity of particles. Temperature of dust grains depends upon the random thermal velocity which is directly related to kinetic energy. Moreover, viscous dissipation effects become important when either the viscosity is larger or when the fluids have a low thermal conductivity, which increases the temperature gradients. One can clearly see the viscous shear heating at shear locations in Fig. 7, in which space dependent temperature profile has been plotted at various times. In these temperature profiles because of spatial period number 3, six maxima (at the location of interface between two consecutive anti parallel flow) show the shear heating locations. As time increases, magnitude of temperature increases and at time $t = 1000\omega_0^{-1}$, temperature
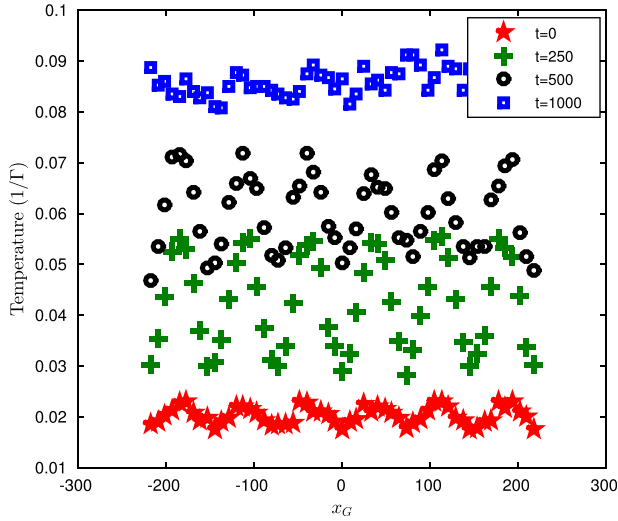
FIG. 7. $\bar{T}(x_G) = \langle \bar{T}(x_G, 0, t) \rangle$, temporal evolution of temperature profile as a function of x for different time for $\Gamma_0 = 50$, equilibrium velocity magnitude $U_0 = 1$, screening parameter $\kappa = 0.5$.

starts to saturate. In Fig. 8, space dependent "fluidizing" velocity profile has been plotted at $y = 0$ axis. Again a clear signal of molecular shear heating is visible, which shows that because of shear heating vorticity structures are destroyed. In Fig. 9, we have plotted average Γ which is inverse of temperature as a function of time. The thermal speed for $\Gamma_0 = 50, 100,$ and 150 are $0.2, 0.14142,$ and 0.11547, respectively, and are much smaller than equilibrium velocity speed $U_0 = 1$ (therefore, the shear heating phenomena occur and result in the decay in Γ value). We find that decay-rate is dependent on equilibrium flow velocity. To better understand the interplay between heat conduction and viscous heating, we define a parameter α which is a ratio of equilibrium speed of shear flow to the thermal speed $\alpha = U_0/v_{th}$.

We divide our observations into three categories:

(a)   [$\alpha = 0.5$ or $(U_0 < v_{th})$]: For this case, the thermal speed is greater than the equilibrium velocity speed. In Fig. 10, shear heating is very small for $\alpha = 0.5$ for various
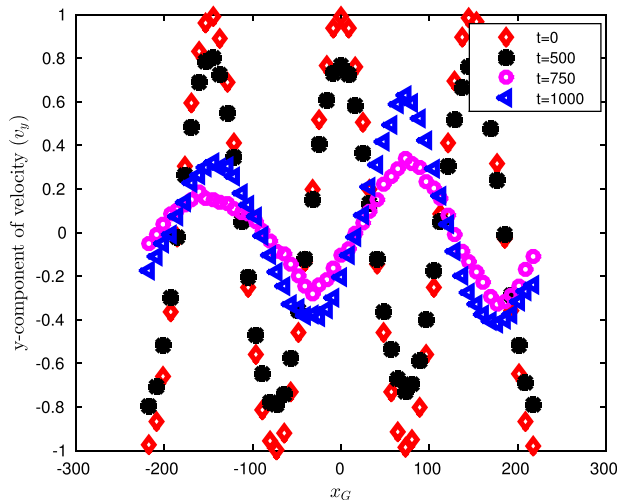

FIG. 9. Spatial average coupling parameter Γ vs time plot for different value of initial Γ_0 for equilibrium velocity magnitude $U_0 = 1$, screening parameter $\kappa = 0.5$ at y = 0 axis.

values of coupling parameter. One can say, that for larger value of thermal speed, the coupling parameter will be constant with very small fluctuations throughout the simulation.

(b)   [$\alpha = 2.0$ or $(U_0 > v_{th})$]: In this case, it is found that the decay rate of higher $\Gamma_0 = 100, 150$ is quite close, however, a slight smaller for $\Gamma_0 = 50$.

(c)   [$\alpha = 6.0$ or $(U_0 \gg v_{th})$]: For this case, the thermal speed is much smaller than the equilibrium velocity speed, results in the faster decay for high $\Gamma_0 = 100,$ 150. For $\Gamma_0 = 100, 150$, decay-rate is close to each other while for $\Gamma_0 = 50$ it is slower compared to the higher Γ_0.

FIG. 8. $v_y(x_G) = \langle v(x_G, 0, t) \rangle$, temporal evolution of velocity profile as a function of x for different time for $\Gamma_0 = 50$, equilibrium velocity magnitude $U_0 = 1$, screening parameter $\kappa = 0.5$.
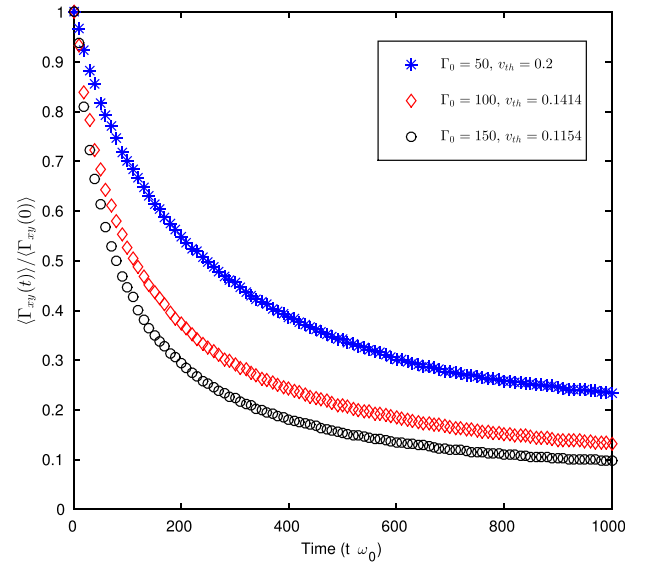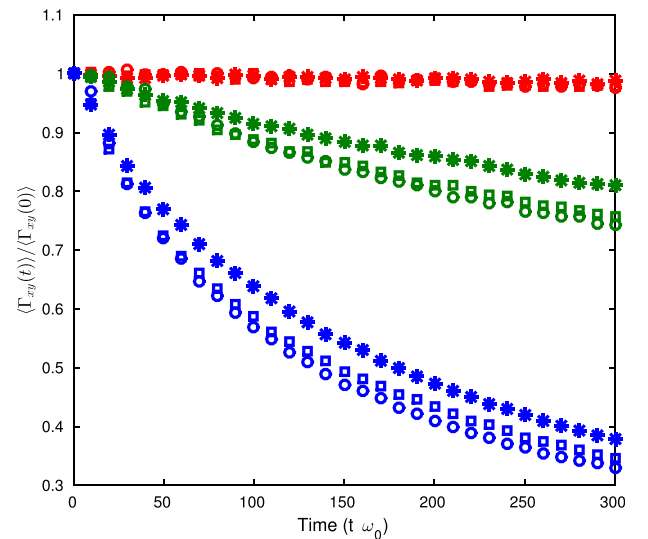

FIG. 10. Spatially averaged coupling parameter $\Gamma(t)$ as a function of time for three different values of initial Γ_0, namely, $\Gamma_0 = 50(*)$, $100(\square)$ and $150(\circ)$. Colors correspond to the cases $\alpha = 0.5$(red), 2(green), and 6 (blue).
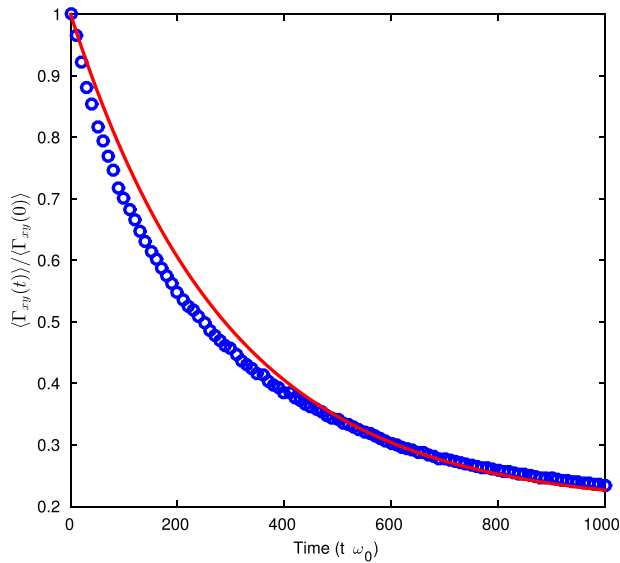
FIG. 11. $\langle \Gamma \rangle_{xy}$ vs time plot for $\Gamma_0 = 50$, equilibrium velocity to thermal velocity ratio, say, $\alpha = U_0/v_{th} = 5$. Fit line is $0.2[1 + 4.0\exp(-\beta t)]$. Calculated decay rate is $\beta = 3.4 \times 10^{-3}$.

In Fig. 11, we have fitted the decay-rate data with an exponentially fit $a[1 + b\exp(-\beta t)]$, where $a = 0.2$, $b = 4.0$, β are intercept, coefficient of exponential part and decay-rate, respectively. β describes how rapidly the coupling parameter decreases as the time increases. The decay rate β of coupling parameter is approximately 3.4×10^{-3} qualitatively. To see the dependency of decay rate on equilibrium velocity to thermal velocity ratio ($\alpha = U_0/v_{th}$), we have plotted decay rate vs α in Fig. 12 for coupling parameter $\Gamma_0 = 50$. It is clear that the decay rate of particular coupling parameter monotonically increases with α value.

V. CONCLUSIONS

In the present work, we have investigated laminar to turbulent transition of Kolmogorov flow in strongly coupled Yukawa liquid using "first principle" based molecular
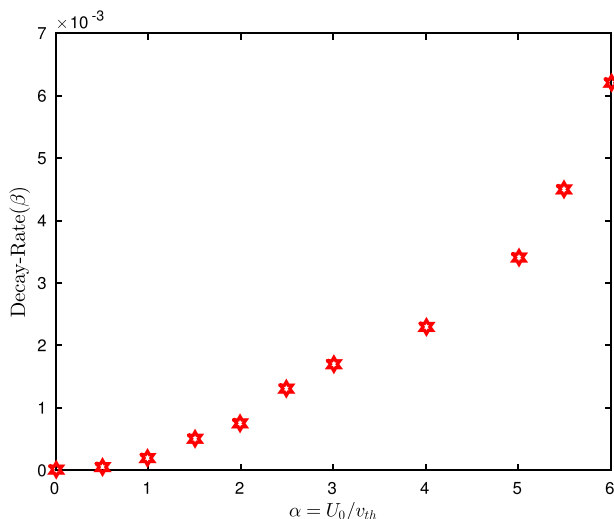

FIG. 12. Decay rate vs $\alpha = U_0/v_{th}$ plot for the number of perturbation mode $m = 2$, coupling parameter $\Gamma_0 = 50$, screening parameter $\kappa = 0.5$, equilibrium spatial period number $n_0 = 3$.

dynamics simulation. Parametric study for range of Reynolds number R has been performed and reveals that the Yukawa liquid in neutral stable state for $R < R_c$ and unstable for $R > R_c$, where R_c is a transition point from where laminar to turbulent transition occurs. The nature of the growth of perturbed mode against Reynolds number exhibits transcritical like bifurcation. We have presented the effect of molecular shear heating on the stability of shear flow in Yukawa liquid. In the early phase, we find that the coupling parameter decays exponentially. At the late times, coherent vortices are destroyed because of molecular shear heating. The description of viscous heating is characterized by space dependent temperature profile at a given coupling parameter ($\Gamma_0 = 50$) of x at $y = 0$ for different times. These space dependent temperature profiles reveal the rise in temperature at shear location. It is also seen that the decay-rate of Γ with time depends upon the ratio of equilibrium shear velocity to thermal velocity. The influence of suppressed molecular shear heating on shear flow to represent the fluid properties without heat dissipation in strongly coupled dusty plasma will be presented in future communication.

[1]P. K. Shukla, N. N. Rao, and M. Y. Yu, Planet. Space Sci. **38**, 543 (1990).
[2]H. Thomas, G. E. Morfill, V. Demmel, J. Goree, B. Feuerbacher, and D. Möhlmann, "Plasma crystal: Coulomb crystallization in a dusty plasma," Phys. Rev. Lett. **73**, 652 (1994).
[3]J. H. Chu and I. Lin, "Direct observation of Coulomb crystals and liquids in strongly coupled rf dusty plasmas," Phys. Rev. Lett. **72**, 4009 (1994).
[4]G. E. Morfill and A. V. Ivlev, "Complex plasmas: An interdisciplinary research field," Rev. Mod. Phys. **81**, 1353 (2009).
[5]V. E. Fortov, V. I. Molotkov, A. P. Nefedov, and O. F. Petrov, "Liquid- and crystallike structures in strongly coupled dusty plasmas," Phys. Plasmas **6**, 1759–1768 (1999).
[6]V. Nosenkol and J. Goree, "Shear flows and shear viscosity in a two dimensional Yukawa system (dusty plasma)," Phys. Rev. Lett. **93**, 155004 (2004).
[7]J. Ashwin and A. Sen, "Microscopic origin of shear relaxation in a model viscoelastic liquid," Phys. Rev. Lett. **114**, 055002 (2015).
[8]H. Ohta and S. Hamaguchi, Phys. Rev. Lett. **84**, 6026 (2000).
[9]H. Ohta and S. Hamaguchi, Phys. Plasmas **7**, 4506 (2000).
[10]J. Ashwin and R. Ganesh, "Kelvin Helmholtz instability in strongly coupled Yukawa liquids," Phys. Rev. Lett. **104**, 215003 (2010).
[11]J. Ashwin and R. Ganesh, "Coherent vortices in strongly coupled liquids," Phys. Rev. Lett. **106**, 135001 (2011).
[12]W.-T. Juan, M.-H. Chen, and I. Lin, "Nonlinear transports and microvortex excitations in sheared quasi-two-dimensional dust Coulomb liquids," Phys. Rev. E **64**, 016402 (2001).
[13]Y. Feng, J. Goree, and B. Liu, "Observation of temperature peaks due to strong viscous heating in a dusty plasma flow," Phys. Rev. Lett. **109**, 185002 (2012).
[14]L. D. Meshalkin and Y. G. Sinai, J. Appl. Math. Mech. **25**, 1700 (1961).
[15]A. M. Obukhov, "Kolmogorov flow and laboratory simulation of it," Russ. Math. Surv. **38**, 113 (1983).
[16]I. Bena, M. Malek Mansour, and F. Baras, "Hydrodynamic fluctuations in the Kolmogorov flow: Linear regime," Phys. Rev. E **59**, 5503 (1999).
[17]D. H. Kelley and N. T. Ouellette, "Using particle tracking to measure flow instabilities in an undergraduate laboratory experiment," Am. J. Phys. **79**, 267 (2011).

[18]V. I. Kliatskin, "On the nonlinear theory of stability of periodic flows," J. Appl. Math. Mech. **36**, 243–250 (1972).

[19]L. D. Landau and E. M. Lifshitz, *Fluid Mechanics* (Pergamon, Oxford, 1984).

[20]J. Ashwin and R. Ganesh, "Effect of external drive on strongly coupled Yukawa systems: A nonequilibrium molecular dynamics study," Phys. Rev. E **80**, 056408 (2009).

[21]G. Salin and J.-M. Caillol, "Transport coefficients of the Yukawa one-component plasma," Phys. Rev. Lett. **88**, 065002 (2002).

[22]S. A. Khrapak and H. M. Thomas, "Fluid approach to evaluate sound velocity in Yukawa systems and complex plasmas," Phys. Rev. E **91**, 033110 (2015).

[23]J. P. Hansen and I. McDonald, *Theory of Simple Liquids: With Applications to Soft Matter*, 4th ed. (Academic, Oxford, 2013).

[24]P. G. Drazin, *Introduction to Hydrodynamic Stability* (Cambridge Text in Applied Mathematics University Press, Cambridge, England, 2002).

[25]J. D. Huba, *NRL Plasma Formulary* (Naval Research Laboratory, Washington, DC, 1994).

[26]A. F. Mills, *Heat and Mass Transfer* (CRC Press, 1995), p. 377.

[27]J. M. White and S. J. Muller, "Viscous heating and the stability of Newtonian and viscoelastic Taylor-Couette flows," Phys. Rev. Lett. **84**, 5130–5133 (2000).

[28]C. P. Tso and S. P. Mahulikar, "Experimental verification of the role of Brinkman number in microchannels using local parameters," Int. J. Heat Mass Transfer **43**, 1837–1849 (2000).

[29]G. Faussurier and M. S. Murillo, "Gibbs Bogolyubov inequality and transport properties for strongly coupled Yukawa fluids," Phys. Rev. E **67**, 046404 (2003).

[30]P. Hartmann, G. J. Kalman, Z. Donkó, and K. Kutasi, "Equilibrium properties and phase diagram of two-dimensional Yukawa systems," Phys. Rev. E **72**, 026409 (2005).